Terahertz Radiation from Nonpolar InN Due to Drift in an Intrinsic In-Plane Electric Field

Grace D. Metcalfe[1*], Hongen Shen[1], Michael Wraback[1], Gregor Koblmüller[2,3], Chad Gallinat[1,2], Feng Wu[2], and James S. Speck[2]

[1] U.S. Army Research Laboratory, Sensors and Electron Devices Directorate, RDRL-SEE-M, 2800 Powder Mill Road, Adelphi, MD 20783, U.S.A.
[2] Materials Department, University of California, Santa Barbara, CA 93106-5050, U.S.A.
[3] Walter Schottky Institut and Physik Department, Technical University Munich, 85748 Garching, Germany

Received July 29, 2010; accepted August 2, 2010; published online August 27, 2010

A sinusoidal dependence of the s- and p-polarized terahertz (THz) emission on sample rotation angle in *m*- and *a*-plane InN has been observed using ultrafast pulse excitation at a moderate pump fluence of ~1 μJ/cm^2. The angular dependence is attributed to carrier drift in an intrinsic in-plane electric field parallel to the *c*-axis induced by stacking fault-terminated internal polarization at wurtzite domain boundaries, with a THz polarity flip corresponding to a reversal of the *c*-axis. The p-polarized THz signal also consists of an angular-independent component, similar to that from *c*-plane InN, consistent with surface normal transport due to the photo-Dember effect. © 2010 The Japan Society of Applied Physics

DOI: 10.1143/APEX.3.092201

Recent interest in nonpolar and semipolar growth orientations to improve device performance by reducing the polarization-induced quantum confined Stark effect in nitride-based optoelectronic devices has also provided new materials for terahertz (THz) applications. In particular, with the correction of the band gap of InN from 2 to ~0.63 eV,[1] nonpolar and semipolar InN is a promising narrow-band-gap semiconductor for efficient THz radiation sources operating at fiber laser wavelengths (1030 and 1550 nm) to leverage fiber optic technology. THz emission from nonpolar *a*-plane InN at high-excitation fluence (0.2–0.35 mJ/cm^2) has been reported,[2] with the THz generation mechanisms attributed to one associated with an in-plane electric field due to In-N bilayers which is independent of sample orientation as well as weak nonlinear optical processes. However, since the fluence of ultrafast fiber lasers is typically in the μJ/cm^2 range, it is important to examine the THz generation mechanism from nonpolar InN in the moderate-excitation fluence range.

In this paper, we present angular-dependent THz emission from *m*-plane $(1\bar{1}00)$ and *a*-plane $(11\bar{2}0)$ InN at moderate-excitation fluence (~1 μJ/cm^2), which significantly differs from that previously reported for *a*-plane InN at high-excitation fluence. We find that the THz signal from the high-stacking fault (SF)-density nonpolar InN films shows a $\sin\theta$ dependence, where θ is the sample rotation angle about the surface normal, as well as a polarity flip with a reversal of the *c*-axis direction, characteristic of real carrier transport in an in-plane electric field parallel to the *c*-axis. Furthermore, the angle dependence of the p-polarized THz field is shifted 90° from that of the s-polarized THz field, consistent with linearly polarized THz emission associated with lateral carrier transport following the sample rotation. We therefore attribute the dominant THz generation mechanism in nonpolar InN to the drift of photoexcited carriers in strong intrinsic lateral electric fields induced by SF-terminated internal polarization at wurtzite domain boundaries. Only the p-polarized THz signal from nonpolar InN consists of an additional angular-independent component, similar to that observed from *c*-plane (0001) InN, as expected with surface normal transport due to the photo-Dember effect.[3] The term p-polarized (s-polarized) refers to the polarization of the THz waveform parallel (perpendicular) to the plane of incidence [Fig. 1(a)].

The high-quality *m*-plane InN film (~1 μm thick) and *a*-plane InN epilayer (~0.5 μm thick) were grown by plasma-assisted molecular beam epitaxy (PA-MBE) on an SF-free *m*- and *a*-plane GaN substrate from Mitsubishi Chemical, respectively. The *m*-plane (*a*-plane) InN material contains an average SF density of $\sim 0.5\times10^6$ cm^{-1} ($\sim 1\times10^6$ cm^{-1}). Further growth details of the nonpolar InN films can be found in refs. 4 and 5. The *c*-plane InN was grown by PA-MBE on a semi-insulating (Fe-doped) GaN template provided by Lumilog to a thickness of ~2.7 μm.[1] All InN films are optically excited with a 250 kHz Coherent regenerative amplifier (RegA) at 800 nm with an excitation power of 2.5 mW, a ~1 mm^2 spot size, and a typical pulse width of 150 fs. The pump is incident on the samples at 45° to the surface normal, and the subsequent THz radiation is collected with a pair of off-axis parabolic mirrors onto a ZnTe crystal for polarization-sensitive electrooptic sampling.

Figure 1 shows image plots of (b) s- and (c) p-polarized time-resolved THz emission as a function of sample rotation angle θ from the *m*-plane InN film. Only the p-wave THz signal [Fig. 2(c)] is corrected for surface normal transport, as described in ref. 6, since THz radiation from vertical transport is p-polarized and angle-independent.[7] At $\theta = 0°$, the *c*-([0001]) axis is in the plane of incidence [i.e., parallel to the p-polarization detection direction, see Fig. 1(a)]. As demonstrated in the image plots and cross-sectional graphs in Figs. 1(b) and 1(c), at $t = t_0$, the THz amplitude reaches a positive extreme at 270° (180°) and a negative extreme at 90° (0°) when the *c*-axis is parallel or antiparallel to the s-polarization (p-polarization) detection direction. The cross-sectional plots in Fig. 1 at fixed sample rotation angles show a polarity flip of the THz waveform with a reversal in the *c*-axis for both polarizations. A THz signal polarity flip can occur when carriers accelerate in the opposite direction.

The s- (empty circles) and p-polarized (solid circles) THz amplitude at $t = t_0$ from Fig. 1 is plotted as a function of sample rotation angle in Fig. 2. The similar amplitude curves show a $\sin\theta$ dependence as well as a 90° phase shift between the p- and s-wave curves, consistent with a linearly polarized THz field, expressed as $E_0(\sin\theta\mathbf{s} + \cos\theta\mathbf{p})$, rotated by an angle θ. The vectors $\mathbf{s}$ and $\mathbf{p}$ are the s- and p-polarization detection directions, respectively. The measured THz polarization vector is parallel to the *c*-axis

*E-mail address: grace.metcalfe@us.army.mil

 © 2010 The Japan Society of Applied Physics

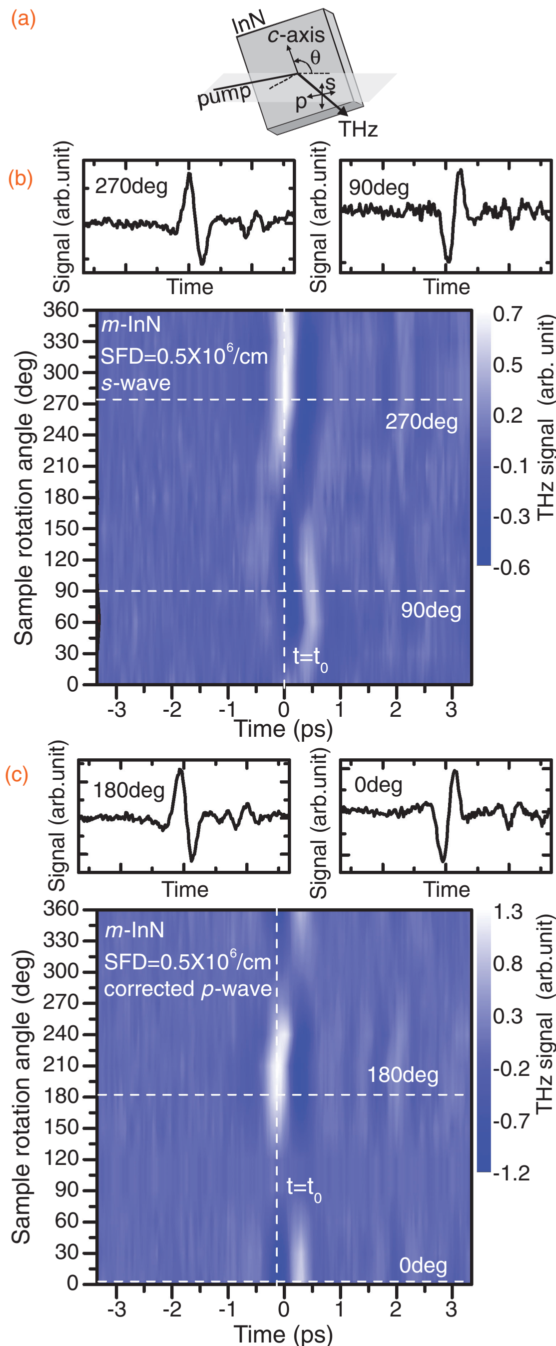

Fig. 1. (a) Schematic of nonpolar InN rotation relative to the emitted THz polarization directions. Image plots of time-resolved (b) s- and (c) p-polarized THz waveforms as a function of sample rotation angle from m-plane InN with an average stacking fault density of ~0.5 x 10^6 cm^{-1} at an excitation fluence of ~1 μJ/cm^2. Cross sections of the image plots at the indicated angles are shown above the image plots. The p-polarized terahertz signal has been corrected for surface normal transport.

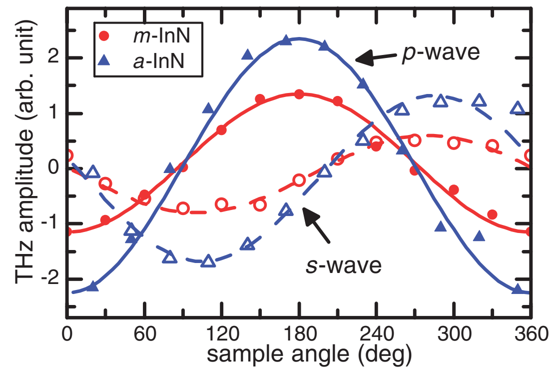

Fig. 2. Plot of p- (solid circles) and s-polarized (empty circles) THz amplitude at $t = t_0$ from m-plane InN data shown in Fig. 1 as a function of sample rotation angle. Equivalent a-plane InN data also shown (triangles). Lines are a $\sin\theta$ (solid) and $\cos\theta$ (dashed) fit to the data.

direction, indicating linearly polarized THz emission due to carrier transport along the c-axis. From the orientation of the c-axis and the corresponding maximum and minimum peak polarized-THz signals, electron acceleration is determined to be along the $[000\bar{1}]$ direction, consistent with carrier transport in a lateral electric field due to SF-terminated internal polarization. Figure 2 also shows that polarized detection of THz emission from a-plane InN exhibits the same angular dependence as m-plane InN.

The angular dependence of the THz emission from nonpolar InN is similar to that due to photoconductive (PC) switches, where the THz emission due to lateral transport is linearly polarized and the polarization follows the orientation of the in-plane electric field as the sample rotates about the surface normal, producing a 90° phase shift between the p- and s-polarized THz emission angular dependence curves. Due to the strong internal polarization in nitride materials,[8,9] the internal electric fields in the nanoscale wurtzite domains can be comparable to those applied to PC switches, with an upper bound unscreened average SF-induced in-plane electric field in the wurtzite region of nonpolar InN with an I_1-type SF density of $1 \times 10^6\,\mathrm{cm}^{-1}$ estimated as $\sim 250\,\mathrm{kV/cm}$, using $P_{\mathrm{sp}} = -0.042\,\mathrm{C/m^2}$,[9] $\varepsilon_{\mathrm{w}} = 15.3$,[10] and $\varepsilon_{\mathrm{zb}} = 15.1$.[11]

Measurements up to an excitation fluence of $\sim 50\,\mu\mathrm{J/cm^2}$ show the same $\sin\theta$ dependence as in Figs. 1 and 2. No optical rectification is observed, because evidence of the nonlinear process in nonpolar nitrides would appear as $a_0 \sin\theta + b_0 \sin(3\theta)$ or $a_1 \sin\theta + b_1 \sin(2\theta)$ for bulk or surface optical rectification,[12] respectively. The 90° phase shift as well as the $\sin\theta$ dependence of the THz field from m- and a-plane InN shown in Fig. 2 differ from the 180° phase shift and $a \sin\theta + b \sin(4\theta)$ dependence reported by Ahn *et al.*[2] for a-plane InN at much higher excitation fluence.

When the c-axis of nonpolar InN is aligned appropriately along the p-polarization direction, in-plane drift can enhance the p-polarized THz amplitude by more than a factor of 2. As mentioned above, the p-polarized THz emission also contains an angle-independent component, which can be isolated and removed. We attribute the angle-independent signal to vertical carrier transport due to the photo-Dember effect, as in c-plane InN.[3]

Figure 3 shows that the time-resolved p-polarized THz emission curves at an excitation fluence of $\sim 1\,\mu\mathrm{J/cm^2}$ from c-plane InN at various sample rotation angles are almost identical. No s-polarized component from c-plane InN is detected. The angle-independent p-polarized THz waveform and the lack of an s-polarized component are consistent with vertical transport in c-plane InN for which the c-axis is normal to the surface. The inset in Fig. 3 shows self-screening effects in a linear-log plot of the peak THz amplitude divided by the pump fluence as a function of

© 2010 The Japan Society of Applied Physics

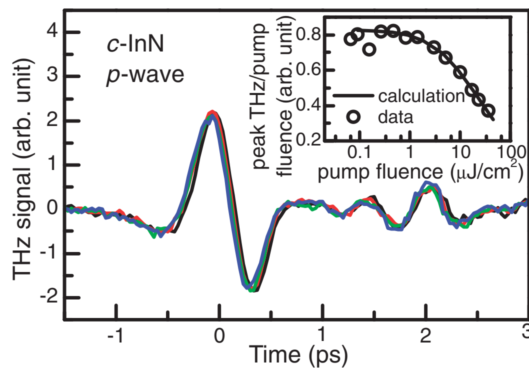

Fig. 3. Time-resolved p-polarized THz waveforms from *c*-plane InN plotted for sample rotation angles ranging from 0 to 360° and an excitation fluence of ~1 μJ/cm². Inset: Plot of measured (circles) and calculated (line) peak THz amplitude divided by pump fluence versus pump fluence.

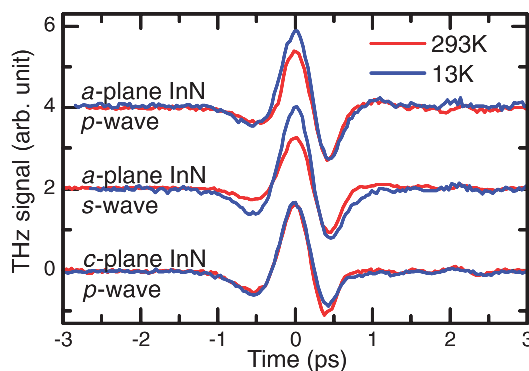

Fig. 4. Time-resolved THz waveforms from *a*- and *c*-plane InN at 13 K (blue) and 293 K (red).

the pump fluence.[13] The solid circles indicate data points measured from *c*-plane InN and the line represents calculations based on drift-diffusion equations incorporating momentum conservation and relaxation. At a pump fluence of $\sim 1\,\mu\text{J/cm}^2$, saturation as well as nonlinear effects should be negligible.

Further insight into the differences between THz generation from nonpolar and *c*-plane InN may be obtained from temperature-dependent measurements, which show an increase in THz signal from *a*-plane InN and a negligible change in THz signal from *c*-plane InN when the temperature is lowered to 13 K (see Fig. 4). The negligible change in THz signal from the *c*-plane InN may be related to the calculation that the donor level in InN is in the conduction band.[14] For the *a*-plane InN, however, the background electrons may become trapped at the stacking faults, which are zincblende inclusions of smaller bandgap, resulting in a reduction of background carriers in the wurtzite domains. At lower temperatures, more background carriers become trapped at the stacking faults and the increased THz signal observed in the *a*-plane InN may therefore be related to reduced screening of the THz signal by the background carriers left in the wurtzite domains. A lowering of background carriers to reduce screening is especially important in InN since the number of background carriers is still high (comparable or higher than *c*-plane InN with a background carrier concentration of $\sim 10^{17}$–10^{18} cm^{-3}) leading to an emitted THz amplitude from nonpolar InN that is ~9 times smaller than that from InAs. Decreasing the background carrier concentration can lead to a more than an order of magnitude increase in emitted THz amplitude from InN.[3]

In summary, we have measured THz emission from *m*- and *a*-plane InN due to drift in lateral electric fields induced by SF-terminated internal polarization at a pump fluence ranging from 1–$50\,\mu\text{J/cm}^2$. The $\sin\theta$ dependence and 90° phase shift between p- and s-polarized THz radiation is consistent with lateral transport in an in-plane electric field parallel to the *c*-axis. The lateral transport in what are effectively arrays of contactless nanoscale PC switches in these nonpolar nitride materials allows for better out-coupling of THz radiation, as in conventional PC switches, without electrode processing and a bias voltage to establish the in-plane electric field. No optical rectification is observed. An angle-independent component is measured only in p-polarized THz emission from nonpolar InN, as well as *c*-plane InN, consistent with surface normal transport. The strong internal polarization, high saturation velocity, large intervalley spacing, short carrier lifetime, and potentially high breakdown field in InN could allow low background concentration nonpolar InN-based THz sources to exploit drift in a SF-induced in-plane electric field and surpass the performance of the semiconductor surface emitter with the highest emission efficiency to date, lightly p-doped InAs.

1) C. S. Gallinat, G. Koblmüller, J. S. Brown, S. Bernardis, J. S. Speck, G. D. Metcalfe, E. D. Readinger, H. Shen, and M. Wraback: Appl. Phys. Lett. **89** (2006) 032109, and references therein.
2) H. Ahn, Y.-P. Ku, C.-H. Chuang, C.-L. Pan, H.-W. Lin, Y.-L. Hong, and S. Gwo: Appl. Phys. Lett. **92** (2008) 102103.
3) G. D. Chern, E. D. Readinger, H. Shen, M. Wraback, C. S. Gallinat, G. Koblmüller, and J. S. Speck: Appl. Phys. Lett. **89** (2006) 141115.
4) G. Koblmüller, A. Hirai, F. Wu, C. S. Gallinat, G. D. Metcalfe, H. Shen, M. Wraback, and J. S. Speck: Appl. Phys. Lett. **93** (2008) 171902.
5) G. Koblmüller, G. D. Metcalfe, M. Wraback, F. Wu, C. S. Gallinat, and J. S. Speck: Appl. Phys. Lett. **94** (2009) 091905.
6) G. D. Metcalfe, H. Shen, M. Wraback, A. Hirai, F. Wu, and J. S. Speck: Appl. Phys. Lett. **92** (2008) 241106.
7) J. D. Jackson: *Classical Electrodynamics* (Wiley, New York, 1999) 3rd ed., p. 661.
8) F. Bernardini, V. Fiorentini, and D. Vanderbilt: Phys. Rev. B **56** (1997) R10024.
9) O. Ambacher, J. Majewski, C. Miskys, A. Link, M. Hermann, M. Eickhoff, M. Stutzmann, F. Bernardini, V. Fiorentini, V. Tilak, B. Schaff, and L. F. Eastman: J. Phys.: Condens. Matter **14** (2002) 3399.
10) V. Bougrov, M. E. Levinshtein, S. L. Rumyantsev, and A. Zubrilov: in *Properties of Advanced Semiconductor Materials: GaN, AlN, InN, BN, SiC, SiGe*, ed. M. E. Levinshtein, S. L. Rumyantsev, and M. S. Shur (Wiley, New York, 2001) p. 49.
11) C. Persson and A. F. da Silva: J. Cryst. Growth **305** (2007) 408.
12) M. Reid and R. Fedosejevs: Proc. SPIE **5577** (2004) 659.
13) Z. Jiang and X.-C. Zhang: in *Sensing with Terahertz Radiation*, ed. D. Mittleman (Springer, Berlin, 2003) p. 159.
14) A. Janotti and C. Van de Walle: Appl. Phys. Lett. **92** (2008) 032104.

© 2010 The Japan Society of Applied Physics